Chemical Science

ROYAL SOCIETY OF CHEMISTRY

EDGE ARTICLE

View Article Online
View Journal | View Issue

Cite this: *Chem. Sci.*, 2024, **15**, 4581

All publication charges for this article have been paid for by the Royal Society of Chemistry

Received 13th January 2024
Accepted 22nd February 2024

DOI: 10.1039/d4sc00276h

rsc.li/chemical-science

Unleashing the high energy potential of zinc–iodide batteries: high-loaded thick electrodes designed with zinc iodide as the cathode†

Jingkang Ma,[ab] Alireza Azizi,[c] Erhuan Zhang,[d] Hong Zhang,*[b] Anqiang Pan *[ce] and Ke Lu *[a]

The realization of high energy is of great importance to unlock the practical potential of zinc–iodine batteries. However, significant challenges, such as low iodine loading (mostly less than 50 wt%), restricted iodine reutilization, and severe structural pulverization during cycling, compromise its intrinsic features. This study introduces an optimized, fully zincified zinc iodide loaded onto a hierarchical carbon scaffold with high active component loading and content (82 wt%) to prepare a thick cathode for enabling high-energy Zn–I_2 batteries. The synergistic interactions between nitrogen heteroatoms and cobalt nanocrystals within the porous matrix not only provide forceful chemisorption to lock polyiodide intermediates but also invoke the electrocatalytic effects to manipulate efficient iodine conversion. The ZnI_2 cathode could effectively alleviate continuous volumetric expansion and maximize the utilization of active species. The electrochemical examinations confirm the thickness-independent battery performance of assembled Zn–I_2 cells due to the ensemble effect of composite electrodes. Accordingly, with a thickness of 300 μm and ZnI_2 loading of up to 20.5 mg cm^{-2}, the cathode delivers a specific capacity of 92 mA h $g_{cathode}^{-1}$ after 2000 cycles at 1C. Moreover, the Zn–I_2 pouch cell with ZnI_2 cathode has an energy density of 145 W h $kg_{cathode}^{-1}$ as well as a stable long cycle life.

Introduction

Aqueous zinc–iodine (Zn–I_2) batteries are promising candidates for large-scale energy storage devices due to their notable attributes, such as high energy/power density, enhanced safety, low cost, and wide availability.[1–5] However, the scalable application potentials of Zn–I_2 batteries are still compromised by some key inherent problems associated with iodine cathodes, such as limited utilization of active components and the significant volumetric expansion of iodine during repeated discharging/recharging processes.[6–10] While engineering the composition and/or structure of composite iodine cathodes provides possible solutions to increase iodine utilization, there is a trade-off in cathode materials between specific capacity and active materials content, thereby compromising the available specific energy of Zn–I_2 cells.[11–21] According to the latest findings in the available research, the introduction of inactive host materials usually decreases the content of active components (mostly less than 60 wt%), which is significantly different from the necessary conditions for high content in practical composite cathodes (>80 wt%, Fig. 1a).[22–26] Furthermore, the structural stability of the iodine cathode plays a pivotal role in determining the cycling life of the assembled practical cells. However, the conventional iodine cathode based on elemental iodine species suffers from a volume expansion of 30.84% in the first zincification. This imposes substantial stress on the host materials, which can lead to cracking and structural pulverization and/or collapse of the cathodes (Fig. 1b).[27–30] For this purpose, replacing iodine with fully zincified zinc iodide (ZnI_2) paves an attractive pathway for solving the above problem because it experiences a volume shrinkage of 23.52% during dezincification, providing space for subsequent volume expansion of the zincification. Such merit minimizes the structural destruction of the composite cathode and may allow higher loading of ZnI_2 compared with I_2. Moreover, apart from improving the utilization and stability of the cathode, a thick electrode design has been considered a direct and promising solution to elevate the energy density of cells to reach the practical level this is attributed to its ability to provide much

[a]*Institutes of Physical Science and Information Technology, Key Laboratory of Structure and Functional Regulation of Hybrid Materials of Ministry of Education, Anhui University, Hefei, Anhui 230601, China. E-mail: luke@ahu.edu.cn*

[b]*School of Chemistry and Chemical Engineering, Harbin Institute of Technology, Harbin, Heilongjiang 150001, China. E-mail: zhanghonghit@hit.edu.cn*

[c]*School of Materials Science and Engineering, Central South University, Changsha 410083, Hunan, China. E-mail: pananqiang@csu.edu.cn*

[d]*Global Institute of Future Technology, Shanghai Jiao Tong University, Shanghai 200240, China*

[e]*School of Physics and Technology, Xinjiang University, Urumqi, Xinjiang, 830046, China*

† Electronic supplementary information (ESI) available. See DOI: https://doi.org/10.1039/d4sc00276h

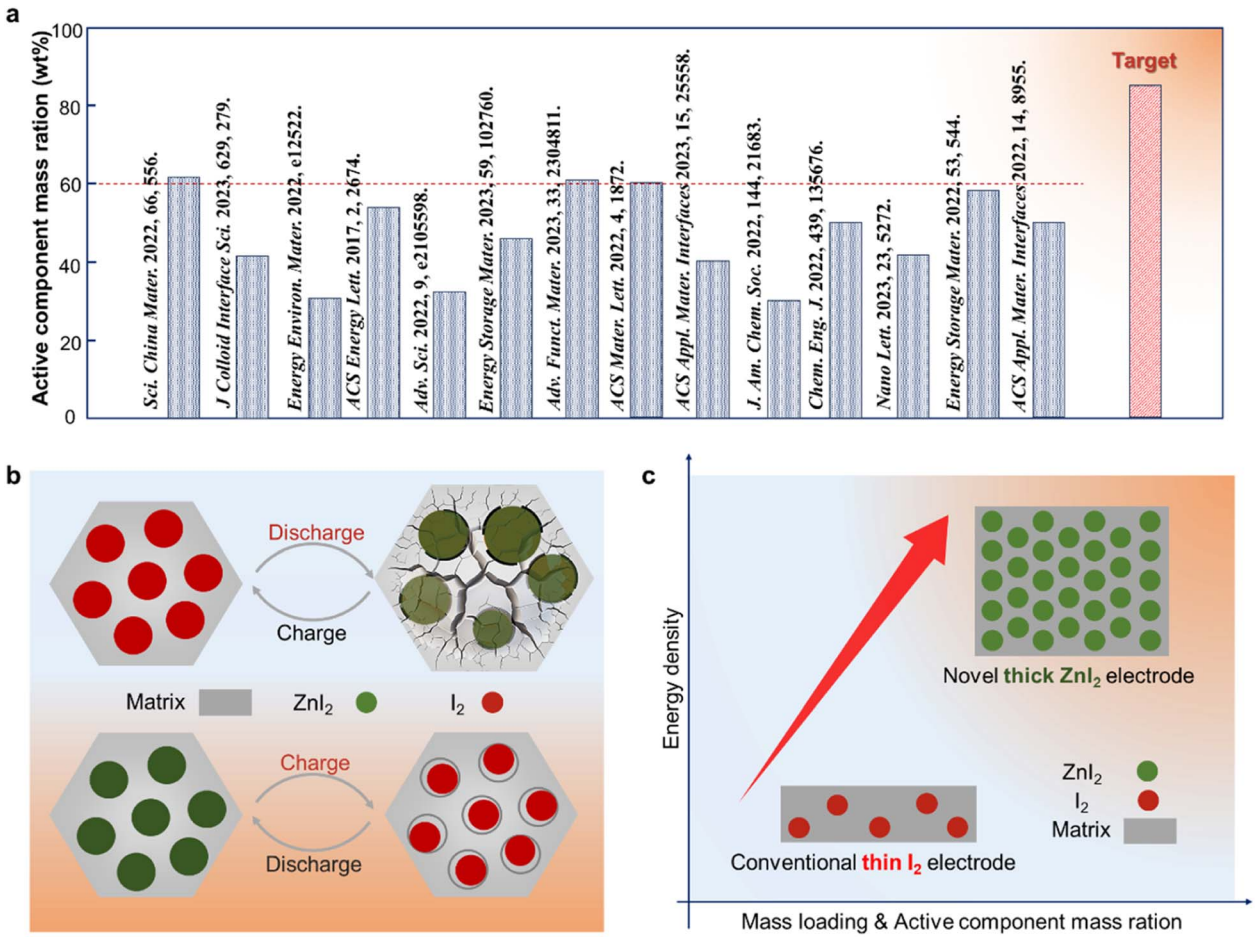

Fig. 1 Schematic of the possible solutions to unlock the high-energy potentials of zinc–iodine electrochemistry. (a) The iodine mass ration in previously reported composite cathodes that were used to assemble zinc–iodine batteries and desired active species content in the practical composite cathode. (b) Schematic for the structural change of composite materials in which the iodine and fully zinced ZnI_2 are active species during the charge and discharge process. (c) Schematic illustrations of the design strategy for realizing the high energy-density zinc–iodine batteries.

space to enhance the energy density of given electrochemically coupled cells *via* maximizing the volume ratio of active to inactive materials.[31–33] However, based on our current knowledge, the construction of thick electrodes for Zn–I_2 batteries has not been reported. Therefore, compared with conventional thin I_2 electrodes, it is hypothesized that using well-designed high-loading ZnI_2 cathodes with high content and iodine utilization to fabricate the thick electrodes is a feasible approach to achieve high-energy-density Zn–I_2 batteries (Fig. 1c). Herein, we report the realization of high-energy Zn–I_2 batteries utilizing hierarchical cobalt nanocrystals decorated carbon as the bifunctional matrix for supporting fully zincified ZnI_2 with high content up to 82 wt% as novel thick cathodes. The synergistic interactions between heteroatoms and metal nanocrystals not only allow strong physicochemical immobilization of intermediate iodine species but also invoke the electrocatalytic effect to manipulate efficient iodine reversible conversion. Significantly, unlike I_2 cathodes, benefiting from the initial shrinkage of the fully zinced ZnI_2 cathode during dezincification, the critical issue of continuous volumetric expansion directed irreversible structural pulverization and/or collapse during long cycling can be alleviated within the thick electrode. Notably, the electrochemical examinations confirm the thickness-independent battery performance of assembled Zn–I_2 cells due to the ensemble effect of composite electrodes. Accordingly, these features enable the ZnI_2 cathode, with an areal mass loading of up to 20.5 mg cm^{-2} and a thickness of 300 μm, to achieve a high capacity of 92 mA h $g_{cathode}^{-1}$ after 2000 cycles at 1C. Meanwhile, a proof-of-concept pouch cell using the ZnI_2 cathode delivers an energy density of 145 W h $kg_{cathode}^{-1}$ along with a stable long cycle life. Our work offers a novel insight for developing advanced cathodes to realize practical zinc–iodine electrochemistry.

Results and discussion

Structural characterization of the functional matrix

Fig. 2a shows the schematic illustration of the preparation process of NC-Co. Initially, the ZIF-8 nanoparticles were synthesized at room temperature through a standard

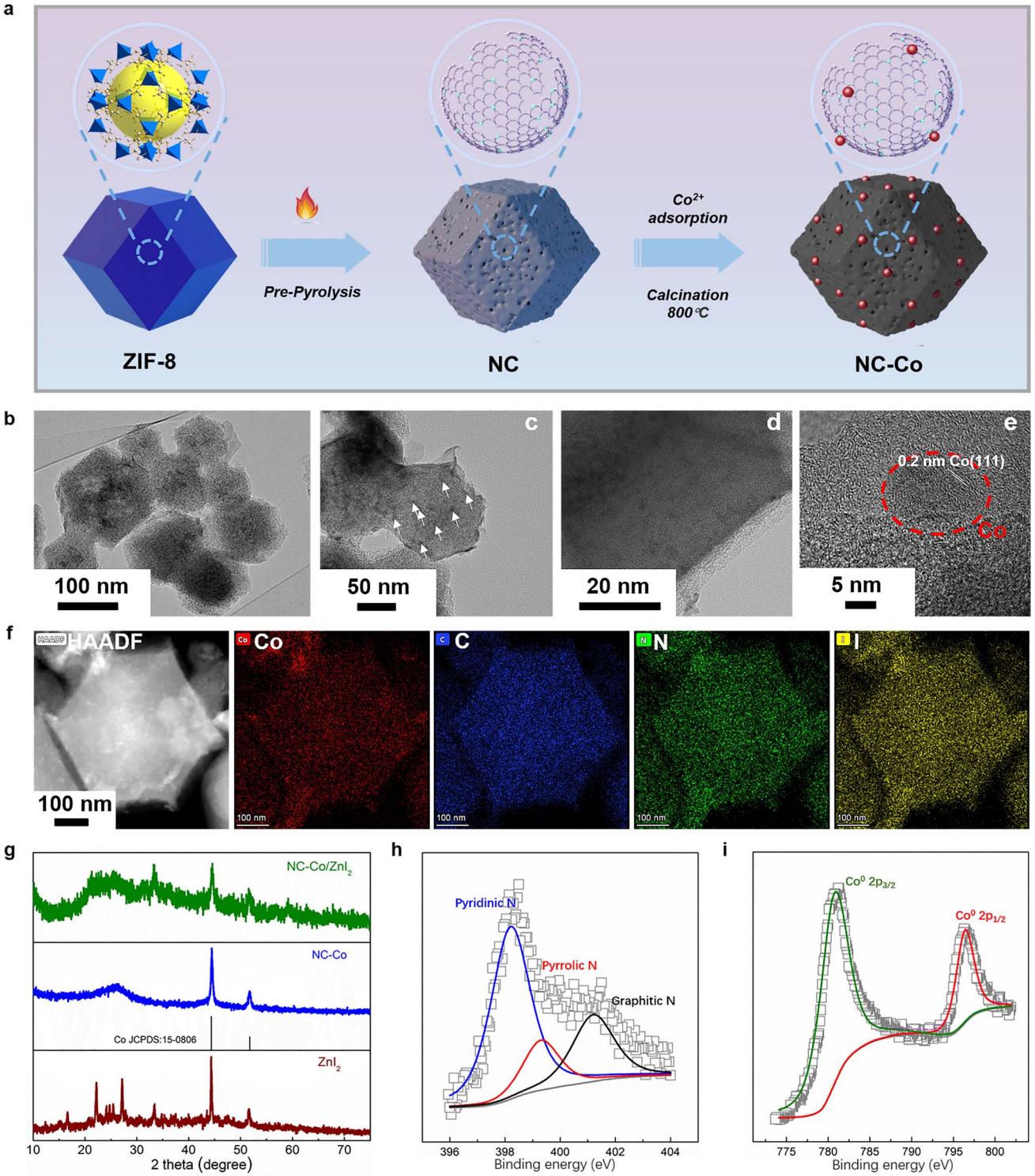

Fig. 2 Schematic illustration and structural characterization of bifunctional NC-Co matrix. (a) The schematic diagram for the synthesis of NC-Co. (b–e) TEM images of the NC-Co. (f) HAADF-STEM of NC-Co/ZnI_2 and the corresponding elemental mapping of Co, C, N, and I. (g) XRD patterns of different samples as noted. High-resolution XPS spectra of (h) N 1s and (i) Co 2p for NC-Co.

method.[34,35] Subsequently, the porous N-doped carbon (NC) was prepared through the direct pyrolysis of ZIF-8 under the N_2 atmosphere. Following that, the NC powder was dispersed in $Co(NO_3)_2$ solution to gain the precursor that filled with Co(II) in nanopores.[36] After the second thermal activation of this precursor in nitrogen/hydrogen flow, the final product named NC-Co was obtained. The transmission electron microscope (TEM) images of the NC-Co are shown in Fig. 2b–e, where it still

maintains a regular rhombic dodecahedral morphology. The highly porous structure and uniformly loaded nanoparticles are clearly observed (Fig. 2c, arrows represent the positions of nanoparticles). High-resolution TEM (HRTEM) shows lattice stripes with a spacing of 0.2 nm, which is consistent with the spacing of the (111) plane of Co, further suggesting that these particles are in the form of monolithic Co nanocrystals and anchored on the NC framework.[37–39] As shown in Fig. 2f, HAADF-STEM images and the corresponding EDX elemental maps reveal the uniform distribution of C, N, Co, I elements in the NC-Co composites after ZnI_2 loading and further confirm that the ZnI_2 was loaded in the pores of the NC-Co rather than randomly attached on the interface. The X-ray powder diffraction (XRD) patterns of ZnI_2, NC-Co, and NC-Co/ZnI_2 samples are presented in Fig. 2g. Notably, the NC-Co/ZnI_2 composite exhibits the crystal peaks of ZnI_2, which is consistent with the fact that zinc iodide is uniformly dispersed in the nanopores of the NC-Co framework. In addition, the valence states and compositions of the elements of NC-Co have been studied by X-ray photoelectron spectroscopy (XPS). The resolved N 1s spectrum (Fig. 2h) displays the coexistence of graphite (401.2 eV), pyrrole (400.1 eV), and pyridine (398.6 eV), implying that N has been successfully doped into the carbon matrix.[40,41] The two prominent peaks at 780.9 and 796.5 eV in the Co 2p spectrum (Fig. 2i) are assigned to metallic Co, suggesting that the Co species in NC-Co are present as metal states rather than oxidized states.[42]

Investigation of the bifunctional matrix manipulated reversible iodine conversion

High loading of active substances is a prerequisite for realizing high-energy Zn–I_2 batteries. The nitrogen adsorption–desorption isotherms (Fig. 3a) are used to investigate the structural information of NC-Co, NC-Co/I_2, and NC-Co/ZnI_2. As shown, the NC-Co exhibits typical type IV isotherms, hysteresis returns, as well as the presence of high nitrogen adsorption at low pressures, suggesting the coexistence of micropores and mesopores in its structure.[43,44] Following iodine impregnation, there is a significant decrease in the N_2 adsorption characteristics in the low-pressure region, while the hysteresis return line still exists in the high-pressure region. Comparatively, the minimization of the nitrogen adsorption profile characteristics at both low and high pressures is almost achieved with loaded ZnI_2. In addition, calculations performed by Brunauer–Emmert–Teller (BET) show that the specific surface area of NC-Co/ZnI_2 (34 $m^2\ g^{-1}$) is significantly lower than that of NC-Co/I_2 (186 $m^2\ g^{-1}$) and NC (988 $m^2\ g^{-1}$), suggesting that the ZnI_2 is fully encapsulated within the micropores/mesopores of NC-Co compared to I_2. The corresponding pore size distributions in Fig. 3b further indicate that the multistage pore structure of NC-Co provides more space for loading high contents of ZnI_2 and enables complete infiltration of ZnI_2 into its pores, which is consistent with the nitrogen adsorption isotherm. Moreover, NC-Co with abundant polar nitrogen and cobalt sites can enhance the intermolecular interaction force with the same polar molecule ZnI_2 through intermolecular dipole–dipole interactions, thus realizing the ZnI_2 chemisorption and obtaining a higher content of ZnI_2 loading. For these reasons, the zinc iodide realizes loadings of up to 82% (Fig. 3c and S1†).

To evaluate the chemical anchoring capability of NC-Co towards polyiodide and the stability of different cathodes during the reaction, the color of the electrolytes for the three electrodes has been compared in the visual vial experiments, as shown in Fig. 3d. It is clearly observed that the color of the electrolyte of the cell with NC-Co/ZnI_2 cathode remains colorless after the cycling test, while the electrolyte in the NC-Co/I_2 cell turns light yellow, and the color change is even more obvious in the AC/ZnI_2 cell. On the one hand, the difference between NC-Co/ZnI_2 and AC/ZnI_2 is attributed to the chemical affinity of NC-Co towards polyiodides, which can better confine the release of soluble polyiodides. On the other hand, the continuous volume expansion of iodine during cycling and the serious dissolution in the electrolyte result in ineffective locking of polyiodides by the NC-Co/I_2 cathode, which exhibits deeper electrolyte color as compared with the NC-Co/I_2 cathode. The results of the UV-visible spectra in Fig. 3e further quantified the above speculation.[45] As shown, the NC-Co/I_2 exhibits much lower absorption peak intensity (0.17) at ~365 nm compared to AC/ZnI_2 (0.41). Encouragingly, the absorption peak of NC-Co/ZnI_2 is negligible. This suggests that the synergistic of ZnI_2 and NC-Co promise efficient active species confinement. Furthermore, *in situ* Raman characterization has been conducted to validate the matrix catalytic effect of NC-Co/ZnI_2 in Zn–I_2 batteries. Initially, the bands at 110 and 164 cm^{-1} are attributed to the symmetric stretching bands of I_3^- and I_5^-, respectively.[46–48] For the NC-Co/ZnI_2 electrode (Fig. 3f), the peak intensities of I_3^- and I_5^- increase with the increase of potential during charging and reach the maximum intensity at 1.6 V. During the discharge process, the peak intensities of I_3^- and I_5^- gradually decrease with decreasing the potential, ultimately disappear completely until the discharge potential of approximately 0.4 V. The NC-Co/ZnI_2 electrode displays a gradual conversion of iodide ($I_5^- \leftrightarrow I_3^- \leftrightarrow I^-$) as well as excellent reversibility under the charging and discharging potentials. In contrast, during charge/discharge, the incomplete conversion of iodine intermediates within the NC/ZnI_2 electrode (Fig. 3g) indicates sluggish kinetics in the reversible conversion of iodine, thus leading to lower conversion efficiency. The strong catalytic effect of the Co catalytic center promotes rapid iodine redox conversion and simultaneously strengthens the inhibition of the polyiodide shuttle (Fig. 3h).

Electrochemical investigation on the cathodic component dependent battery performance

The electrochemical measurements were performed to estimate the effect of the cathodic component on the electrochemical performance of Zn–I_2 cells. Note that the majority of composite iodine cathodes in existing investigations incorporate significant amounts of inactive substrates (even up to 50 wt%) to improve the iodine utilization, but diminish the specific energy. Therefore, to obtain practically relevant results, all the specific capacities and current densities are normalized based on the

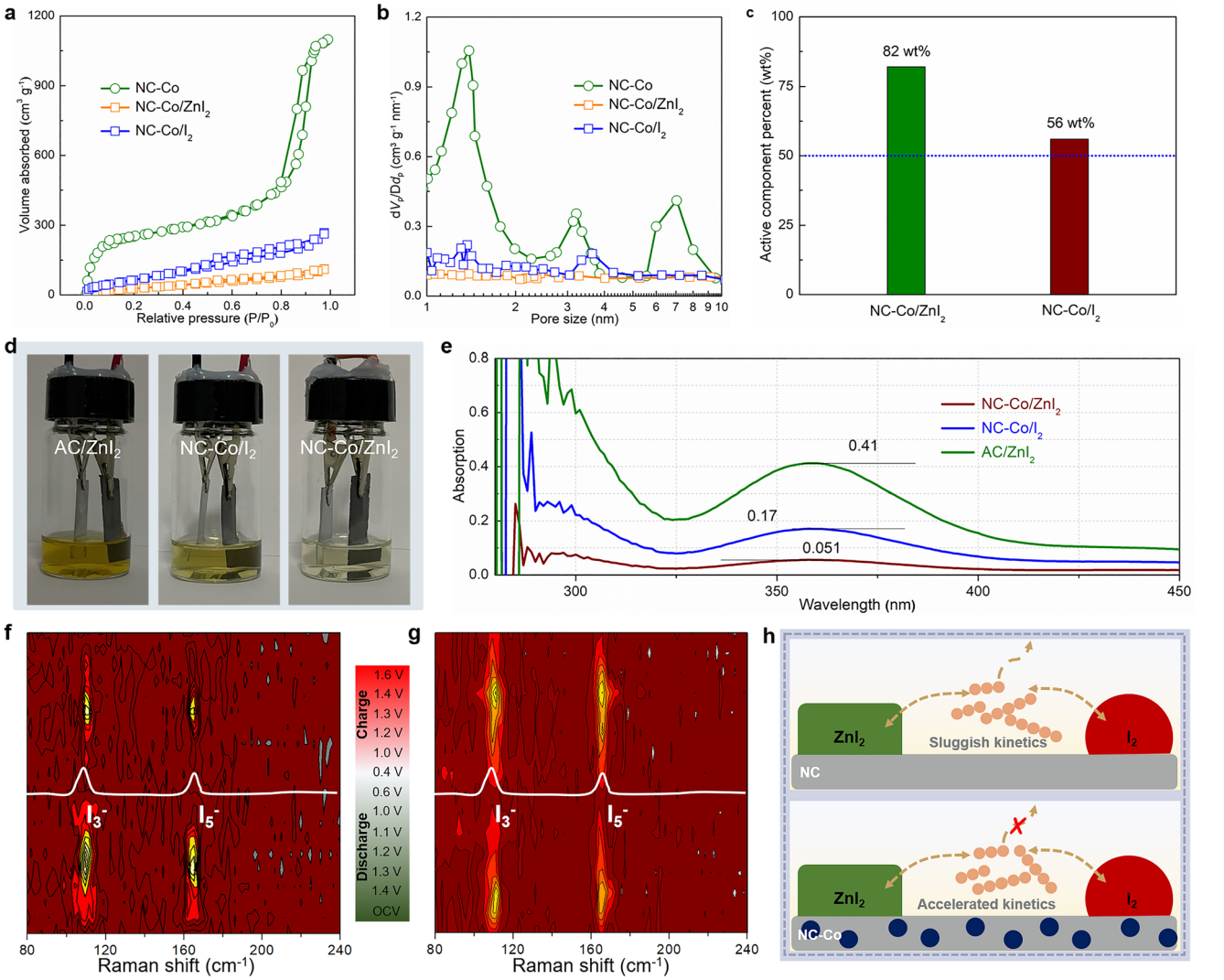

Fig. 3 Mechanistic investigation on the reversible iodine speciation pathway. (a) Nitrogen adsorption–desorption isotherms and (b) corresponding pore size distributions of the NC-Co, NC-Co/I_2, and NC-Co/ZnI_2. (c) Active component percents in the NC-Co/I_2 and NC-Co/ZnI_2 composites. (d) Photographs of Zn–I_2 batteries with AC/ZnI_2, NC-Co/I_2, and NC-Co/ZnI_2 cathodes after the cycling stability test. (e) UV-vis absorption spectra of the electrolyte in (d). *In situ* Raman spectra of (f) NC-Co/ZnI_2 and (g) NC/ZnI_2 electrodes at different discharge/charge states. (h) Schematic illustration of the matrix-dependent tunable iodine conversion efficiency.

mass of composite cathodes in cells. As shown in Fig. 4a, the AC/ZnI_2 delivers a specific capacity of 84 mA h g^{-1} at 1C (1C = 167 mA g^{-1}), while the introduction of heteroatom catalytic centers can achieve a 28.6% capacity increase (108 mA h g^{-1} of NC/ZnI_2). The implantation of Co hotspots intensifies this pattern, as verified by the notably higher capacity exhibited in NC-Co/ZnI_2 (130 mA h g^{-1}) when compared to control electrodes. It is noteworthy that the NC-Co/I_2 presents a high specific capacity of 180 mA h g^{-1} based on the mass of the active component, which is higher than the NC-Co/ZnI_2 (150 mA h g^{-1}). However, when calculating specific capacity based on the composite cathode, the capacity sharply decreases to 90 mA h g^{-1} and is only comparable with the AC/ZnI_2 (Fig. 4b). It should be noted that the NC-Co matrix alone without ZnI_2 loading have neglectable contribution to the total capacity (Fig. S2†). This significant difference not only highlights the importance of evaluating specific capacity based on the mass of the overall cathode but also confirms the high active component content in maximizing battery performance toward the practical application.

The improved cycling stability has been a persistent challenge for Zn–I_2 cells, whose structural pulverization of the cathode is caused by continuous volumetric variation during the charging/discharging. Interestingly, using the ZnI_2 as the cathodic material addresses this concern. As a proof-of-concept experiment, both the NC-Co/ZnI_2 and NC-Co/I_2 electrodes, with the same active materials loading (~3 mg cm^{-2}), performed 100 cycles at 1C. The corresponding SEM analysis was conducted on the cathodes before and after cycling. As shown in Fig. 4c and d, the thickness of the NC-Co/ZnI_2 electrode remains nearly unchanged after the cycle, whereas the electrode thickness of NC-Co/I_2 experiences an expansion rate of about 52.4%. Such

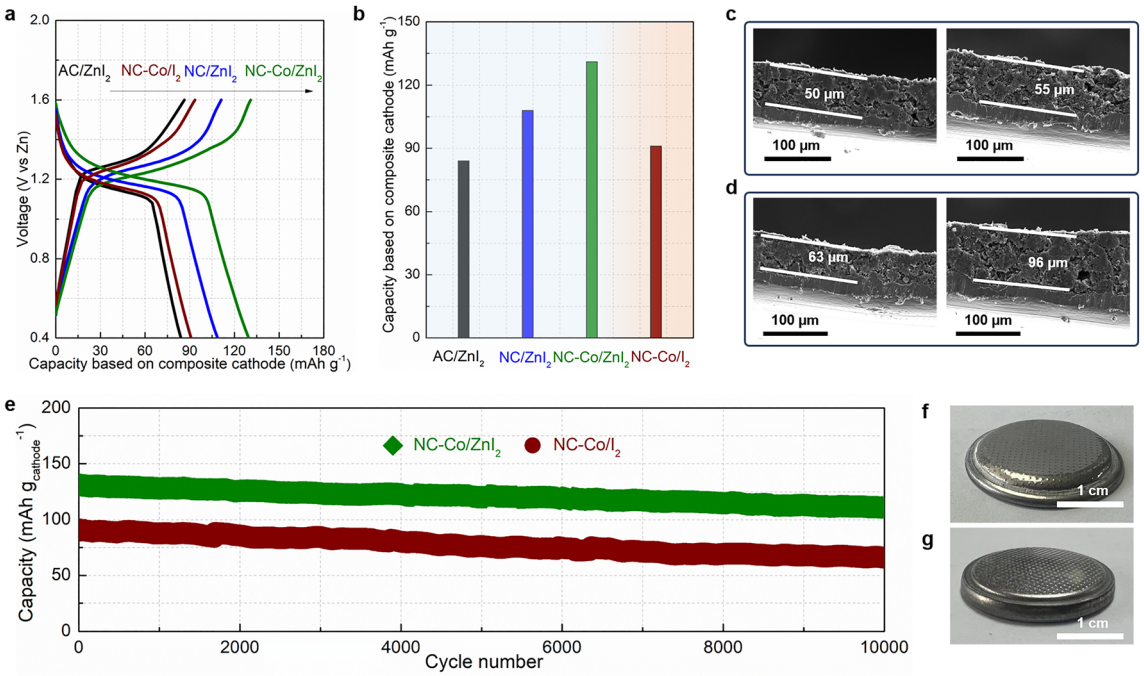

Fig. 4 Electrochemical performance of the ZnI_2-based composite electrodes. (a) Voltage–capacity profiles and (b) the specific capacities of AC/ZnI_2, NC-Co/I_2, NC/ZnI_2, and NC-Co/ZnI_2 electrodes with the active component loading of 3 mg cm^{-2} for Zn ion storage at 1C. (c) Cycling stability of Zn–I_2 cells with different cathodes as noted. Cross-sectional SEM images of (d) NC-Co/ZnI_2 and (e) NC-Co/I_2 cathodes before and after 100 cycles test. Photographs of (f) NC-Co/I_2//Zn and (g) NC-Co/ZnI_2//Zn cells after cycling tests in (c).

differences reveal that the initial shrinkage of the ZnI_2 cathode during dezincification could minimize the continuous volumetric expansion and maintain the high stability of the electrode. Accordingly, the NC-Co/ZnI_2 indeed exhibits enhanced cycling stability compared to the NC-Co/I_2. Specifically, the NC-Co/ZnI_2 cathode allows high-capacity retention of 85.4% after ultra-long cycling over 10 000 cycles at 1C, which is better than the limited capacity retention of 72.1% for the NC-Co/I_2 electrode (Fig. 4e), highlighting the cathodic component-dependent battery performance. By comparison with some representative reports, the NC-Co/ZnI_2 cathode demonstrates an outstanding cycling life and competitive specific capacity based on the mass of the composite cathode (Table S1†). Meanwhile, visually, the coin cell with NC-Co/I_2 cathode exhibits significant swelling, as depicted in Fig. 4f after the cycling test, while in contrast, there is no observable change in the NC-Co/ZnI_2//Zn cell (Fig. 4g), confirming the superiority of ZnI_2 as the cathodic material. Moreover, the superior rate capability indicates that the active ZnI_2 not only could stabilize the cathode structure but also endow the faster redox kinetics. As shown in Fig. S3,† when the current density is increased 10 times to 10C, the NC-Co/ZnI_2 still realizes a high-capacity retention of 79.2%, which is far more than the 47.1% retention observed in NC-Co/I_2.

Thickness-independent battery performance of the Zn–I_2 cells using high-loading electrodes

To improve the energy efficiency of Zn–I_2 cells for practical applications, the electrochemical performance of NC-Co/ZnI_2 electrodes with different thicknesses is also investigated. Fig. 5a–c show cross-sectional SEM images of NC-Co/ZnI_2 cathodes compacted with ZnI_2 loadings of 6.8 mg cm^{-2}, 12.8 mg cm^{-2}, and 20.5 mg cm^{-2}, respectively, which correspond to electrode thicknesses of 100, 200 and 300 μm. As shown in Fig. 5d, even at such high area loading, the capacity of NC-Co/ZnI_2 still exhibits initial capacities of 120, 115, and 108 mA h $g_{cathode}^{-1}$, which are much higher than those of NC-Co/I_2 under the same conditions (79, 56, and 45 mA h $g_{cathode}^{-1}$). In the cycling performance (Fig. 5e and f), after 2000 cycles, NC-Co/ZnI_2 exhibits a reversible capacity of 107 mA h $g_{cathode}^{-1}$ for the area mass loading of 6.8 mg cm^{-2}, 102 mA h $g_{cathode}^{-1}$ for 12.8 mg cm^{-2}, 92 mA h $g_{cathode}^{-1}$ for 20.5 mg cm^{-2}. In contrast, NC-Co/I_2 experiences severe degradation during cycling, providing only the capacity of 52, 27, and 16 mA h $g_{cathode}^{-1}$. Meanwhile, NC-Co/ZnI_2 can maintain almost the same capacity retention at different area loads, whereas the capacity retention of NC-Co/I_2 consistently decreases with increasing mass loading (Fig. 5g), which indicates that the increased thickness of the NC-Co/ZnI_2 electrode does not influence cell performance. In addition, NC-Co/I_2 cells at different area loads exhibit severe swelling after cycling (Fig. 5h). In contrast, cells with NC-Co/ZnI_2 display minimal volume changes, underscoring the fact that ZnI_2 facilitates the mitigation of volume expansion during cycling. Finally, a pouch cell with NC-Co/ZnI_2 cathode is assembled further to demonstrate its practical application in the Zn–I_2 system (Fig. 5i). The initial coulombic efficiency is about 94.7% for the first cycle. After the first cycle, the coulombic efficiency reaches 98.3% and a record-high average CE of 99.1% after 100 cycles. Note that the pouch cell exhibits an

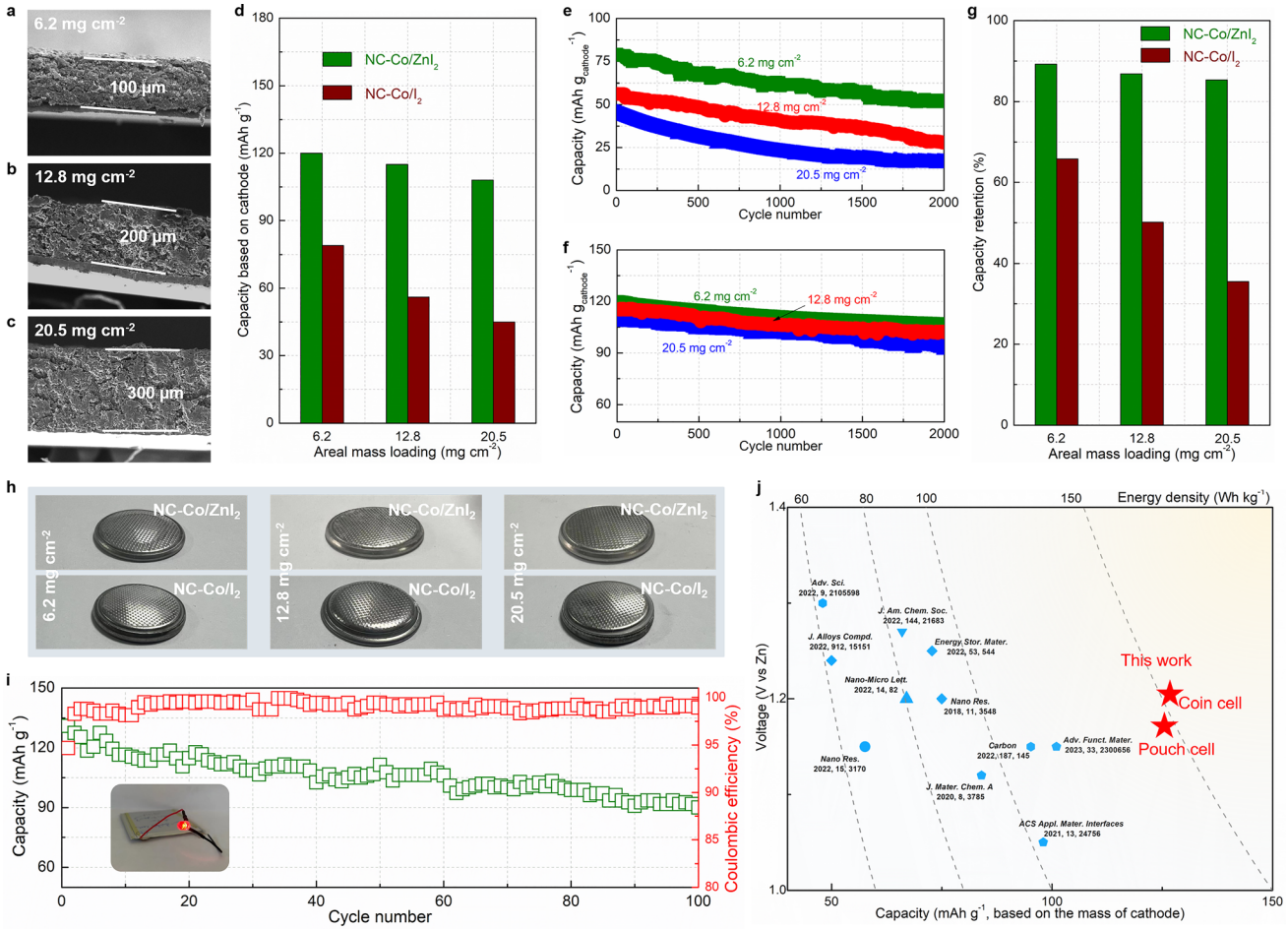

Fig. 5 Electrochemical performance of ZnI_2 assembled Zn–I_2 cells with high active component loading. (a–c) Cross-sectional SEM images of thick NC-Co/ZnI_2 electrodes with different area mass loading. (d) Comparison of capacities for NC-Co/ZnI_2 and NC-Co/I_2 cathodes with varied loading contents. Long-term cycling performance of the (e) thick NC-Co/I_2 and (f) thick NC-Co/ZnI_2 cathodes. (g) The capacity retention of the NC-Co/I_2 and NC-Co/ZnI_2 electrodes in (e and f) after 2000 cycles. (h) Digital photos of the post-cycled cells with NC-Co/ZnI_2 and NC-Co/I_2 at various areal mass loadings. (i) The cycling performance of NC-Co/ZnI_2//Zn pouch cell, inset is a red LED bulb that can be lighted by a charge Zn–I_2 pouch cell. (j) Overall electrochemical contrast between the published research and the iodine cathode was reported in this work.

initial energy density of 145 W h $kg_{cathode}^{-1}$, and provides a reversible capacity of 90 mA h g^{-1} after 100 cycles, and it also displays the capability to power a red LED bulb (Fig. 5i, inset), further demonstrating the viability of the NC-Co/ZnI_2 cathode for utilization in realistic devices. Actually, the influence of the weight of the anode and electrolyte on the calculation of the energy density of full cells was considered. Lowering the mass loading of metal anode (thin metal anode and low N/P ratio) and E/S ratio are very important for the real application of batteries. Accordingly, the pouch cells assembled with different E/S ratios and the same cathodes were further tested and the results are shown in Table S2.† In accordance, the stability decreases with lower E/S and N/P ratios. Based on all of these aspects, we believe the content of electrolyte determine the upper limit of overall energy density of pouch cell. For future research, lean-electrolyte cells and/or novel electrolyte that could realize the tunable/efficient iodine conversion are need to be explored. Fig. 5j provides a comprehensive comparison of the Zn–I_2 cells (coin and pouch) produced in this work with those previously reported studies. The cells in this study exhibit the highest energy density and discharge capacity, confirming the reliability and practicability of the reported system.

Conclusion

In summary, we present a practical high-energy Zn–I_2 battery that utilizes fully zinced iodide as active components. Hierarchically, cobalt nanocrystals and nitrogen heteroatom decorated carbon were fabricated and used as polar matrix to realize an extremely high active component loading and reaching up to 82 wt%. The introduction of dual catalytic hotspots not only facilitates strong physicochemical immobilization of poly(-iodide) intermediates but also manipulates deep and reversible iodine conversion, even after a long cycling test. Experiment results confirm that the ZnI_2-based cathodic materials could minimize the continuous volumetric expansion/shrinkage and permit the high reutilization of the active species simultaneously. The ensemble effect of composite electrodes enables

the thickness-independent battery performance of as-prepared Zn–I_2 cells. Accordingly, the thick cathodes with high ZnI_2 loading of up to 20.5 mg cm^{-2} and thickness of 300 μm exhibit a high capacity of 92 mA h $g_{cathode}^{-1}$ after 2000 cycles at 1C. Furthermore, the stable Zn–I_2 pouch cell with an energy density of 145 W h $kg_{cathode}^{-1}$ was also demonstrated, highlighting its potential for practical applications.

Data availability

Data available on request.

Author contributions

K. L. conceived and designed the project. J. M. and H. Z. performed all experimental and mechanism studies and wrote the required scripts. All authors were involved in the analysis of the results and further editing and reviewing process.

Conflicts of interest

The authors declare no competing financial interests.

Acknowledgements

This work was financially supported by the Natural Scientific Foundation of China (22109001, 22208335), Postdoctoral Fellowship Program of CPSF (GZB20230950), and Heilongjiang Postdoctoral Science Foundation (LBH-Z23187).

References

1 M. L. Wang, J. K. Ma, H. Zhang, L. Fu, X. L. Li and K. Lu, *Small*, 2023, (1613–6810), 2307021.
2 L. Q. Zhang, H. L. Guo, W. Zong, Y. P. Huang, J. J. Huang, G. J. He, T. X. Liu, J. Hofkens and F. L. Lai, *Energy Environ. Sci.*, 2023, **16**, 4872–4925.
3 J. Z. Ma, M. M. Liu, Y. L. He and J. T. Zhang, *Angew. Chem., Int. Ed.*, 2021, **60**, 12636–12647.
4 Y. Lyu, J. A. Yuwono, P. T. Wang, Y. Y. Wang, F. H. Yang, S. L. Liu, S. L. Zhang, B. F. Wang, K. Davey, J. F. Mao and Z. P. Guo, *Angew. Chem., Int. Ed.*, 2023, **62**, e202303011.
5 Y. H. Kang, G. H. Chen, H. M. Hua, M. H. Zhang, J. Yang, P. X. Lin, H. Y. Yang, Z. H. Lv, Q. L. Wu, J. B. Zhao and Y. Yang, *Angew. Chem., Int. Ed.*, 2023, **62**, e202300418.
6 L. T. Ma, Y. R. Ying, S. M. Chen, Z. D. Huang, X. L. Li, H. T. Huang and C. Y. Zhi, *Angew. Chem., Int. Ed.*, 2021, **60**, 3791–3798.
7 C. Prehal, H. Fitzek, G. Kothleitner, V. Presser, B. Gollas, S. A. Freunberger and Q. Abbas, *Nat. Commun.*, 2020, **11**, 4838.
8 Z. Cheng, H. Pan, F. Li, C. Duan, H. Liu, H. Y. Zhong, C. C. Sheng, G. J. Hou, P. He and H. S. Zhou, *Nat. Commun.*, 2022, **13**, 6788.
9 Z. G. Li, X. H. Wu, X. Y. Yu, S. Y. Zhou, Y. Qiao, H. S. Zhou and S. G. Sun, *Nano Lett.*, 2022, **22**, 2538–2546.
10 W. W. Zhang, M. L. Wang, H. Zhang, L. Fu, W. L. Zhang, Y. P. Yuan and K. Lu, *Chem. Sci.*, 2023, **14**, 12730–12738.
11 D. L. Yu, A. Kumar, T. A. Nguyen, M. T. Nazir and G. Yasin, *ACS Sustain. Chem. Eng.*, 2020, **8**, 13769–13776.
12 L. J. Yan, T. F. Liu, X. M. Zeng, L. Sun, X. H. Meng, M. Ling, M. Q. Fan and T. L. Ma, *Carbon*, 2022, **187**, 145–152.
13 Q. Guo, H. Z. Wang, X. T. Sun, Y. N. Yang, N. Chen and L. T. Qu, *ACS Mater. Lett.*, 2022, **4**, 1872–1881.
14 H. L. Pan, B. Li, D. H. Mei, Z. M. Nie, Y. Y. Shao, G. S. Li, X. H. S. Li, K. S. Han, K. T. Mueller, V. Sprenkle and J. Liu, *ACS Energy Lett.*, 2017, **2**, 2674–2680.
15 S. Chen, Y. L. He, S. Y. Ding and J. T. Zhang, *J. Phys. Chem. C*, 2023, **127**, 7609–7617.
16 K. Zhang, Q. Yu, J. Sun, Z. Tie and Z. Jin, *Adv. Mater.*, 2023, **36**, 2309838.
17 L. Ma, G. Zhu, Z. Wang, A. Zhu, K. Wu, B. Peng, J. Xu, D. Wang and Z. Jin, *Nano Lett.*, 2023, **23**, 5272–5280.
18 Y. Zhang, L. Wang, Q. Li, B. Hu, J. Kang, Y. Meng, Z. Zhao and H. Lu, *Nano-Micro Lett.*, 2022, **14**, 208.
19 J. Wei, P. Zhang, T. Shen, Y. Liu, T. Dai, Z. Tie and Z. Jin, *ACS Energy Lett.*, 2022, **8**, 762–771.
20 Y. Feng, Y. Wang, L. Sun, K. Zhang, J. Liang, M. Zhu, Z. Tie and Z. Jin, *Small*, 2023, 2302650.
21 X. Guo, S. Liu, X. Wan, J. Zhang, Y. Liu, X. Zheng, Q. Kong and Z. Jin, *Nano Lett.*, 2022, **22**, 4879–4887.
22 A. Bhargav, J. R. He, A. Gupta and A. Manthiram, *Joule*, 2020, **4**, 285–291.
23 K. Lu, Z. Y. Hu, J. Z. Ma, H. Y. Ma, L. M. Dai and J. T. Zhang, *Nat. Commun.*, 2017, **8**, 527.
24 X. Y. Yang, H. Q. Fan, F. L. Hu, S. M. Chen, K. Yan and L. T. Ma, *Nano-Micro Lett.*, 2023, **15**, 126.
25 G. H. Chen, Y. H. Kang, H. Y. Yang, M. H. Zhang, J. Yang, Z. H. Lv, Q. L. Wu, P. X. Lin, Y. Yang and J. B. Zhao, *Adv. Funct. Mater.*, 2023, **33**, 2300656.
26 J. He, H. Hong, S. Hu, X. Zhao, G. Qu, L. Zeng and H. Li, *Nano Energy*, 2024, (119), 109096.
27 C. Bai, F. S. Cai, L. C. Wang, S. Q. Guo, X. Z. Liu and Z. H. Yuan, *Nano Res.*, 2018, **11**, 3548–3554.
28 L. Q. Zhang, M. J. Zhang, H. L. Guo, Z. H. Tian, L. F. Ge, G. J. He, J. J. Huang, J. T. Wang, T. X. Liu, I. P. Parkin and F. L. Lai, *Adv. Sci.*, 2022, **9**, 2105598.
29 H. Chen, X. Li, K. Q. Fang, H. Y. Wang, J. Q. Ning and Y. Hu, *Adv. Energy Mater.*, 2023, **13**, 2302187.
30 X. L. Li, N. Li, Z. D. Huang, Z. Chen, G. J. Liang, Q. Yang, M. Li, Y. W. Zhao, L. T. Ma, B. B. Dong, Q. Huang, J. Fan and C. Y. Zhi, *Adv. Mater.*, 2021, **33**, 2006897.
31 Z. L. Han, S. P. Li, R. Y. Xiong, Z. P. Jiang, M. J. Sun, W. Hu, L. F. Peng, R. J. He, H. M. Zhou, C. Yu, S. J. Cheng and J. Xie, *Adv. Funct. Mater.*, 2022, **32**, 2108669.
32 S. B. Tu, Z. H. Chen, B. Zhang, X. C. Wang, R. M. Zhan, C. H. Li and Y. M. Sun, *Nano Lett.*, 2022, **22**, 5982–5989.
33 J. Y. Wu, X. Zhang, Z. Y. Ju, L. Wang, Z. Y. Hui, K. Mayilvahanan, K. J. Takeuchi, A. C. Marschilok, A. C. West, E. S. Takeuchi and G. H. Yu, *Adv. Mater.*, 2021, **33**, 2101275.
34 Z. C. Yan, Y. R. Liang, W. B. Hua, X. G. Zhang, W. H. Lai, Z. Hu, W. L. Wang, J. Peng, S. Indris, Y. X. Wang,

S. L. Chou, H. K. Liu and S. X. Dou, *ACS Nano*, 2020, **14**, 10284–10293.
35 X. F. Zhou, Z. X. Yu, Y. Yao, Y. Jiang, X. H. Rui, J. Q. Liu and Y. Yu, *Adv. Mater.*, 2022, **34**, 2200479.
36 J. Z. Li, H. G. Zhang, W. Samarakoon, W. T. Shan, D. A. Cullen, S. Karakalos, M. J. Chen, D. M. Gu, K. L. More, G. F. Wang, Z. X. Feng, Z. B. Wang and G. Wu, *Angew. Chem., Int. Ed.*, 2019, **58**, 18971–18980.
37 Y. Y. Xue, Y. B. Guo, Q. M. Zhang, Z. J. Xie, J. P. Wei and Z. Zhou, *Nano-Micro Lett.*, 2022, **14**, 162.
38 W. Y. Du, K. Q. Shen, Y. R. Qi, W. Gao, M. L. Tao, G. Y. Du, S. J. Bao, M. Y. Chen, Y. M. Chen and M. W. Xu, *Nano-Micro Lett.*, 2021, **13**, 50.
39 J. R. Mou, Y. J. Li, T. Liu, W. J. Zhang, M. Li, Y. T. Xu, L. Zhong, W. H. Pan, C. H. Yang, J. L. Huang and M. L. Liu, *Small Methods*, 2021, **5**, 2100455.
40 T. T. Liu, H. J. Wang, C. J. Lei, Y. Mao, H. Q. Wang, X. He and X. Liang, *Energy Storage Mater.*, 2022, **53**, 544–551.
41 J. T. Zhang, Z. H. Zhao, Z. H. Xia and L. M. Dai, *Nat. Nanotechnol.*, 2015, **10**, 444–452.
42 S. H. Liu, J. Li, X. Yan, Q. F. Su, Y. H. Lu, J. S. Qiu, Z. Y. Wang, X. D. Lin, J. L. Huang, R. L. Liu, B. N. Zheng, L. Y. Chen, R. W. Fu and D. C. Wu, *Adv. Mater.*, 2018, **30**, 1706895.
43 H. Zhang, B. Song, W. W. Zhang, B. W. An, L. Fu, S. T. Lu, Y. W. Cheng, Q. W. Chen and K. Lu, *Angew. Chem., Int. Ed.*, 2023, **62**, e202217009.
44 Y. R. Qi, Q. J. Li, Y. K. Wu, S. J. Bao, C. M. Li, Y. M. Chen, G. X. Wang and M. W. Xu, *Nat. Commun.*, 2021, **12**, 6347.
45 W. Z. Gao, S. T. Cheng, Y. X. Zhang, E. R. Xie and J. C. Fu, *Adv. Funct. Mater.*, 2023, **33**, 2211979.
46 S. J. Zhang, J. N. Hao, H. Li, P. F. Zhang, Z. W. Yin, Y. Y. Li, B. K. Zhang, Z. Lin and S. Z. Qiao, *Adv. Mater.*, 2022, **34**, 2201716.
47 H. J. Yang, Y. Qiao, Z. Chang, H. Deng, P. He and H. S. Zhou, *Adv. Mater.*, 2020, **32**, 2004240.
48 M. M. Liu, Q. W. Chen, X. Y. Cao, D. X. Tan, J. Z. Ma and J. T. Zhang, *J. Am. Chem. Soc.*, 2022, **144**, 21683–21691.